Multi-parameter quantitative magnetic resonance imaging in the early assessment of radiation-induced parotid damage in patients with nasopharyngeal carcinoma following intensity-modulated radiotherapy

XIANHAI ZHANG[1*], ZHIFENG XU[1*], YABIN JIN[2], LINWEN HUANG[1], WENXIU WU[1] and MINGYONG GAO[1]

[1]Department of Radiology; [2]Clinical Research Center, The First People's Hospital of Foshan, Foshan, Guangdong 528000, P.R. China

Received October 17, 2023; Accepted February 12, 2024

DOI: 10.3892/ol.2024.14313

Abstract. The present study aimed to investigate the value of intravoxel incoherent motion imaging (IVIM) and three-dimensional pulsed continuous arterial spin labeling (ASL) in assessing dynamic changes of the parotid gland in patients with nasopharyngeal carcinoma (NPC) following radiotherapy (RT). A total of 18 patients with NPC who underwent intensity-modulated RT were enrolled in the present study. All patients underwent conventional magnetic resonance imaging, plus IVIM and ASL imaging of the bilateral parotid glands within 2 weeks prior to RT, and 1 week (1W) and 3 months (3M) following RT. Pure diffusion coefficient (D), pseudo-diffusion coefficient (D*), perfusion fraction (F) and blood flow (BF) were analyzed. D and BF values were significantly increased from pre-RT to 1W post-RT [change rate: Median (IQR), ΔD_{1W}%: 39.28% (38.23%) and ΔBF_{1W}%: 60.84% (54.88%)] and continued to increase from 1W post-RT to 3M post-RT [55.44% (40.56%) and ΔBF%: 120.39% (128.74%)]. In addition, the F value was significantly increased from pre-RT to 1W post-RT, [change rate: Median (IQR), ΔF_{1W}%: 28.13% (44.66%)], and this decreased significantly from 1W post-RT to 3M post-RT. However, no significant differences were observed between pre-RT and 3M post-RT. Results of the present study also demonstrated that the D* value was significantly decreased from pre-RT to 1W post-RT and 3M post-RT [change rate: Median (IQR), $\Delta D^*_{1w\%}$: -41.86% (51.71%) and ΔD^*_{3M}: -29.11% (42.67%)]. No significant difference was observed between the different time intervals post-RT. There was a significant positive correlation between percentage change in ΔBF1W and radiation dose (ρ=0.548, P=0.001). Thus, IVIM-diffusion-weighted imaging and ASL may aid in the detection and prediction of radiation-induced parotid damage in the early stages following RT. They may contribute to further understanding the potential association between damage to the parotid glands and patient-/treatment-related variables, through the assessment of individual microcapillary perfusion and tissue diffusivity.

Correspondence to: Dr Zhifeng Xu, Department of Radiology, The First People's Hospital of Foshan, 81 Lingnan Avenue, Foshan, Guangdong 528000, P.R. China
E-mail: xuzf83@126.com

*Contributed equally

Abbreviations: NPC, nasopharyngeal carcinoma; RT, radiotherapy; IMRT, intensity modulated RT; MRI, magnetic resonance imaging; 3D-pCASL, three-dimensional pulsed continuous arterial spin labeling; DWI, diffusion-weighted imaging; IVIM, intravoxel incoherent motion imaging; ASL, arterial spin labeling; BF, blood flow; ROIs, regions of interest

Key words: IVIM, ASL, RT, parotid gland, NPC

Introduction

Xerostomia caused by gland radiation injury is a common complication of radiotherapy (RT) in patients with nasopharyngeal carcinoma (NPC) that adversely affects long-term quality of life. Studies have confirmed that the degree of glandular functional impairment is highly correlated with radiation dose (1,2). Therefore, modern RT techniques, such as conformal RT, intensity modulated RT (IMRT) and salivary gland preservation, are used to minimize radiation-mediated damage to the parotid gland. In addition, specific drugs are also used to protect the microstructure of the parotid gland, to minimize functional damage, thereby reducing the symptoms of dry mouth (3). However, treatment remains inadequate, and further investigations into alternative strategies are required to improve the protection of the parotid tissue. In addition, further understanding of the mechanisms and evolution of radiation injury of the parotid gland during the whole course of RT is required, particularly in the acute phase. Notably, a decline in gland function due to radiation damage is reversible during the acute phase (4). Results of previous studies demonstrated that inflammation, edema, degeneration and necrosis of

acinus cells, vascular injury and organ atrophy occurred in the glandular tissues of rats, pigs and rhesus monkeys following radiation exposure (4,5). Due to the invasive nature of parotid tissue biopsies and the lack of comprehensive access to the complete glandular tissue damage, similar studies in human subjects are not possible. Therefore, it is of great clinical value to develop *in vivo* techniques for monitoring radiation damage of the parotid gland at both cellular and vascular levels.

Quantitative functional magnetic resonance imaging (MRI) is used for accurately and non-invasively determining microscopic changes in radiation damage in glands. For example, diffusion and perfusion MRI technology accurately provide multiple quantitative indicators associated with tissue biology, such as cell density and vascular perfusion (6,7). Dynamic contrast-enhanced (DCE) MRI (8) is a well-established technique for evaluating hemodynamic characteristics of various tissues, such as vascular leakage and permeability. However, DCE MRI is limited, as the injection of contrast media may cause renal impairment and renal fibrosis. Three-dimensional pulsed continuous arterial spin labeling (3D-pCASL) technology safely and non-invasively evaluates tissue perfusion without the use of a contrast agent. Instead, freely diffusing water molecules are used as endogenous contrast agents (9). Diffusion-weighted imaging (DWI) provides insights into the cellular structure and is sensitive to the heat-driven motion of water molecules in tissues (6). Therefore, DWI accurately reflects the state of radiation-induced cell inactivation. Intrixel incoherent motion imaging (IVIM) is a further development of DWI, capable of delivering both diffusion and perfusion imaging results without the need for contrast injection, with the advantage of being completely non-invasive (9,10). IVIM has been widely used in hepatic fibrosis evaluation (11), staging (9,10), efficacy evaluation (12), the differential diagnosis of fibrosis, and monitoring of NPC recurrence following RT (13).

In January 2019, a prospective study of IVIM and 3D-pCASL was established to assess the tumor response to IMRT in patients with NPC. As part of this ongoing study, the effects of radiation damage to the parotid gland were investigated following treatment. The present study aimed to investigate the effects of radiation damage to the parotid gland in a total of 18 patients.

Materials and methods

Patients. In total, 22 patients with NPC who were diagnosed using nasopharyngeal endoscopy and pathology in The First People's Hospital of Foshan(Guangdong, China) from January 2019 to July 2019 were included in the present study, and the corresponding data were collected. The inclusion criteria were as follows: i) All patients were diagnosed for the first time and had not received any treatment (chemotherapy or chemoradiotherapy); ii) patients had no history of other parotid diseases; and iii) there were no MR examination contraindications. Patients were excluded from the present study according to the following criteria: i) The presence of other head and neck tumors; ii) a history of factors affecting the function of the parotid gland, including mumps, rheumatic immune disease, a history of tumor chemotherapy or secretory disease; iii) poor image quality; and iv) poor compliance (Including the intake of acidic food within 1 h of MR examination). In total, 4 patients were excluded from the present study. Notably, 2 cases exhibited artifacts on imaging, 1 case failed to be re-examined within the specified time period, and 1 patient consumed a carbonated drink 15 min prior to examination. Thus, 18 patients (14 men and 14 women; age range, 34-56 years; median age, 50 years) with NPC were included in the present study, leading to data being available for a total of 36 parotid glands. The detailed clinical information of all patients is displayed in Tables I and SI. Tumor staging was carried out according to the staging standard of the eighth edition of the American Joint Committee on Cancer guidelines (14).

Table I. Selected patient and tumor characteristics.

Characteristic	Value
Patients (parotid glands), n	18 (36)
Sex (male/female), n	14/4
Median age (IQR), years	49.50 (12)
T stage, n (%)	
T1	0 (0.00)
T2	9 (50.00)
T3	3 (16.67)
T4	6 (33.33)
N stage, n (%)	
N0	1 (5.56)
N1	7 (38.89)
N2	7 (38.89)
N3	3 (16.67)
M stage	
M0	18 (100.00)
Clinical stage	
II-III	11 (61.11)
IV	7 (38.89)
Radiation dose, mGy	
Median (IQR)	3715.65 (477.02)
Range	3076.50-6897.50

This prospective study was carried out in accordance with the latest version of the Declaration of Helsinki and was approved by the Ethics Committee of The First People's Hospital of Foshan [approval no. 2018 (18th)]. Written informed consent was obtained at the time of the first MR examination from each patient.

Chemoradiotherapy regimen. According to the China Nasopharyngeal Cancer Staging 2017 Edition (15), all enrolled patients exhibited disease stages II-IVA. Three stages of induction chemotherapy were performed in all patients, followed by radical concurrent chemoradiotherapy plus targeted therapy, in which RT was performed with head and neck IMRT. The total gross dose of the tumor was 70 mGy, the segmentation dose was 2.12 mGy and the number of segmentations was 33. Chemotherapeutic agents were administered prior to RT (docetaxel, 60 mg/m^2, intravenous drip; Nedaplatin (SinopOD: H20064294, specification: 10 mg/branch) 60 mg/m2,

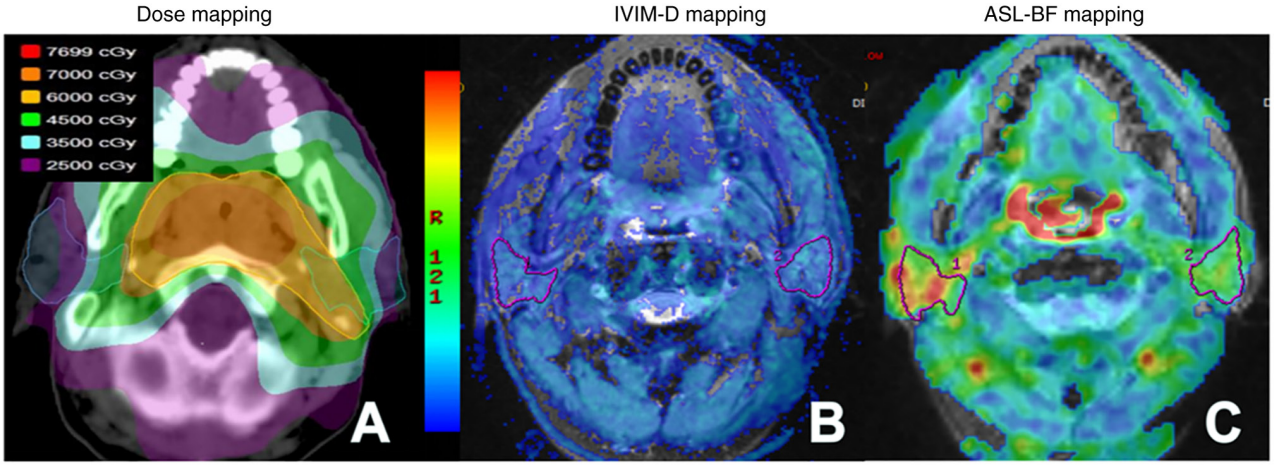

Figure 1. Radiation dose profile and parotid region of interest mapping on IVIM and ASL images. (A) Radiation dose profile, (B) Region of interest profile of IVIM and (C) region of interest profile of ASL. IVIM, intravoxel incoherent motion imaging; D, pure diffusion coefficient; BF, blood flow; ASL, arterial spin labeling.

intravenous drip; 21 days as a course of treatment, continuous treatment for 2 courses.

Radiation dosage data acquisition. The RT regimen for all patients was based on CT positioning images. Patients wore a thermoplastic body membrane of the head, neck and shoulder in a supine position, and were positioned in the Philips 16-row large-aperture spiral CT simulation machine (Philips Healthcare). The scanning range spanned from the top of the head to ~2 cm below the edge of the clavicle, and the thickness of the image layer was ~3 mm. Localized CT images and 3D-T1 Bravo images obtained during pre-treatment scans of patients were transferred to the treatment planning system (Varian Eclipse version 10.0; Varian Medical Systems, Inc.). CT location images were fused with the MR 3D-T1 Bravo images using the automatic matching function. Two nasopharyngeal radiotherapists delineated the target area on the fusion image. Mean and maximum doses were obtained (Fig. 1A).

MRI protocols. Examinations were performed using a 3.0T MR scanner (Discovery 750w 3.0T MR system; Cytiva) and an 8-channel head-and-neck combined coil. The conventional MR examination included the T1-weighted imaging fluid-attenuated inversion recovery sequence as follows: Time of repetition (TR), 657 msec; time of echo (TE), 24 msec; time of inversion, 780 msec; a fat-saturated T2WI fast spin echo (FSE)-based sequence; TR/TE, 5,114/110 msec; number of excitations (NEX), 2.0; field of view (FOV), 240x240 mm; matrix, 288x224; and section thickness/gap, 5/1 mm.

IVIM-DWI was performed using 13 b-values (0, 10, 20, 40, 60, 100, 120, 160, 200, 400, 600, 800 and 1,000 sec/mm^2), and applied using the following single-shot spin echo echoplanar imaging sequence: TR, 3,685 msec; TE, 43 msec; NEX, 2.0; FOV, 240x240 mm; matrix, 160x160; and section thickness/gap, 5/0 mm. For 3D-pCASL, an ASL sequence with a 3D FSE spiral acquisition was performed using the following parameters: TR, 4,295 msec; TE, 11.5 msec; NEX, 3.0; section thickness/gap, 3/0 mm; layer number, 30; FOV, 220x220 mm; matrix, 288x192; post Label Delay (PLD) time, 1,025 msec; and scanning time, 4 min 10 sec. Axial T2WI-FSE was performed using a scanning range and positioning line consistent with those of ASL, and the following additional parameters: TR/TE, 3,000/68 msec. All patients underwent conventional MRI, IVIM and ASL imaging of the bilateral parotid glands within 2 weeks prior to RT and 1 week and 3 months following RT.

The consumption of food or drink was not permitted for at least 1 h prior to MR examination.

MRI data analysis. The IVIM and ASL raw data obtained from scans were transferred to GE-AW 4.6 workstation software (GE Healthcare) for post-processing. Three parameters, namely, pure diffusion coefficient (D), pseudo-diffusion coefficient (D*) and perfusion fraction (F), were automatically derived and calculated from IVIM, by fitting the MR signal acquired at 13 b-values to a bi-exponential model. Blood flow (BF) was automatically derived and calculated from ASL data. The regions of interest (ROIs) were determined within the largest section of the parotid gland on the fusion diagram, using parameters derived from IVIM or ASL and T2WI. The ROI in the D map included the maximal potential amount of parotid parenchyma, excluding visible parotid ducts and retromandibular veins (Fig. 1B). Additional ROIs were automatically matched on D* and F maps. Selection of the ROI in ASL-BF images was consistent with the parameter images of IVIM (Fig. 1C). To improve the accuracy of the ROI outline, all images were enlarged 2-3 times. The change rates of ASL-BF and IVIM (D, D* and F) parameters were calculated using the following equation: $\Delta R(T)\% = (Rpost\text{-}RT - Rpre\text{-}RT)/Rpre\text{-}RT \times 100$, where R represents BF, D, D* and F; and T represents time.

Measurements of all MR parameters were performed by two radiologists with 8 and 12 years of experience in head and neck radiology, respectively. Both radiologists were blinded to the clinical data of the patients and were not aware of the aims of the present study. In total, two doctors reviewed the images and measured the data, and all image analyses and parameter measurements were consistent.

Statistical analysis. Statistical analysis was performed using SPSS software (version, 24.0; IBM Corp.). Descriptive

Table II. Dynamic changes of D, D*, F and BF at different follow-up time-points.

Parameters	Pre-RT	1W post-RT	3M post-RT
D, $x10^{-3}$ sec/mm^2	0.77 (0.19)	1.11 (0.39)	1.21 (0.28)
D*, $x10^{-3}$ sec/mm^2	100.05 (28.85)	65.65 (35.08)	69.80 (35.70)
F, %	0.241 (0.10)	0.315 (0.14)	0.256 (0.09)
BF, ml/100 g/min	24.64 (10.46)	42.00 (16.24)	55.75 (26.92)
ΔD, %	-	39.28 (38.23)	55.44 (40.56)
ΔD*, %	-	-41.86 (51.71)	-29.11 (42.67)
ΔF, %	-	28.13 (44.66)	3.30 (40.43)
ΔBF, %	-	60.84 (54.88)	120.39 (128.74)

D, pure diffusion coefficient; D*, pseudo-diffusion coefficient; F, perfusion fraction; BF, blood flow; RT, radiotherapy; 1W, 1 week; 3M, 3 months. Data are presented as Median (IQR).

statistics were used to analyze the demographic data and clinical characteristics of all patients. Numerical data are presented as the mean ± standard deviation when normally distributed. All other data are presented as the median (IQR). Kolmogorov-Smirnov's test was used to determine whether the parameters were normally distributed. The difference in percentage changes of all parameters derived from IVIM and ASL over time were assessed using a repeated measures Kruskal-Wallis test, and the Wilcoxon rank-sum test was then used as the post hoc test, with Bonferroni's correction used to correct P-values. Potential correlations between MR parameters and dose were analyzed using Spearman's correlation coefficient. $P<0.05$ was considered to indicate a statistically significant difference.

Results

Basic information of patients. Among the 18 included patients, all patients successfully underwent the planned therapeutic regimens and follow-up MR examinations. Detailed clinical data of each patient were available in taleS1. No measurements were excluded due to insufficient quality. ASL-BF and multi-parameters of IVIM (D, D* and F) images of bilateral parotid glands of one representative subject pre- and post-RT are displayed in Fig. 2. All patients exhibited different degrees of dry mouth without quantitative grading.

Dynamic changes in D, D, F and BF at different follow-up time-points*. Dynamic changes in D, D*, F and BF values are displayed in Table II and Fig. 3. Results of the present study demonstrated that D and BF values both increased significantly pre-RT to 1 week (1W) post-RT [median change rate: Median (IQR), ΔD_{1W}%: 39.28% (38.23%) and ΔBF_{1W}%: 60.84% (54.88%)], and these continued to increase from 1W post-RT to 3 months (3M) post-RT [change rate: Median (IQR), ΔD%: 55.44% (40.56%) and ΔBF%: 120.39% (128.74%)]. The results of the present study also demonstrated that the parotid F value was significantly increased from pre-RT to 1W post-RT [change rate: Median (IQR), ΔF_{1W}%: 28.13% (44.66%)], and this was significantly decreased from 1W to 3M post-RT. Notably, there were no significant differences in the change rates between pre-RT and 3M post-RT [change rate: Median (IQR), ΔF_{3M}%: 3.30% (40.43%)]. From pre-RT to 1W post-RT and 3 month (3M) post-RT, the parotid D* value was significantly decreased [change rate: Median (IQR), $\Delta D^*_{1w\%}$: -41.86% (51.71%) and ΔD^*_{3M}: -29.11% (42.67%)]. However, no significant differences were observed between different post-RT time intervals.

Correlation between ΔD, ΔD ΔF and ΔBF and RT dose*. Results of the present study demonstrated that there was a significant positive correlation between percentage change in ΔBF_{1W} and radiation dose ($\rho=0.548$; $P=0.001$). Notably, a higher radiation dose was correlated with a larger percentage change in $\Delta BF_{1W.}$ However, the correlation was insignificant between ΔBF_{3M} and radiation dose ($\rho=0.095$). No significant correlations were observed between ΔD, ΔD* and ΔF and radiation dose at the different follow-up time-points (Table III).

Discussion

Salivary gland cells are sensitive to radiation; therefore, a lack of saliva secretion in patients with head and neck tumors following RT may cause a series of complications, such as dry mouth, dysphagia, loss of taste and oral ulcers (16). These symptoms may also affect a patients' quality of life. Results of a previous study revealed that patients with head and neck tumors who received RT experienced a significant reduction in the size of the parotid glands in the early stages following RT, which may be associated with a decrease in the number of gland cells and acinar atrophy (6,7,17,18). In addition to gland cells, vascular endothelial cells have remained the focus of research surrounding radiation-mediated injury, and the results of previous animal experiments demonstrated that radiation reduces the microvessel density of the parotid gland and local blood flow (5,19). The reduction of local tissue perfusion may affect the function of the excretory duct in the parotid gland, thereby affecting the secretion and excretion of saliva. Non-invasive imaging technology is used to accurately determine potential changes in the morphology and function of the salivary glands damaged by radiation, and to aid in determining the pathophysiological mechanisms underlying radiation damage. As the function of the salivary glands and the degree of radiation damage differ between individuals,

Table III. Correlation of radiation dose with change in intravoxel incoherent motion imaging and arterial spin labeling parameters at different follow-up time-points.

Statistic	RT dose	ΔD_{1W}	ΔD_{3M}	ΔD^*_{1W}	ΔD^*_{3M}	ΔF_{1W}	ΔF_{3M}	ΔBF_{1W}	ΔBF_{3M}
ρ	1.00	-0.092	-0.070	-0.233	-0.243	0.242	0.042	0.549	0.283
P-value		0.592	0.685	0.171	0.153	0.156	0.807	0.001	0.095

RT, radiotherapy; D, pure diffusion coefficient; D*, pseudo-diffusion coefficient; F, perfusion fraction; BF, blood flow; 1W, 1 week; 3M, 3 months.

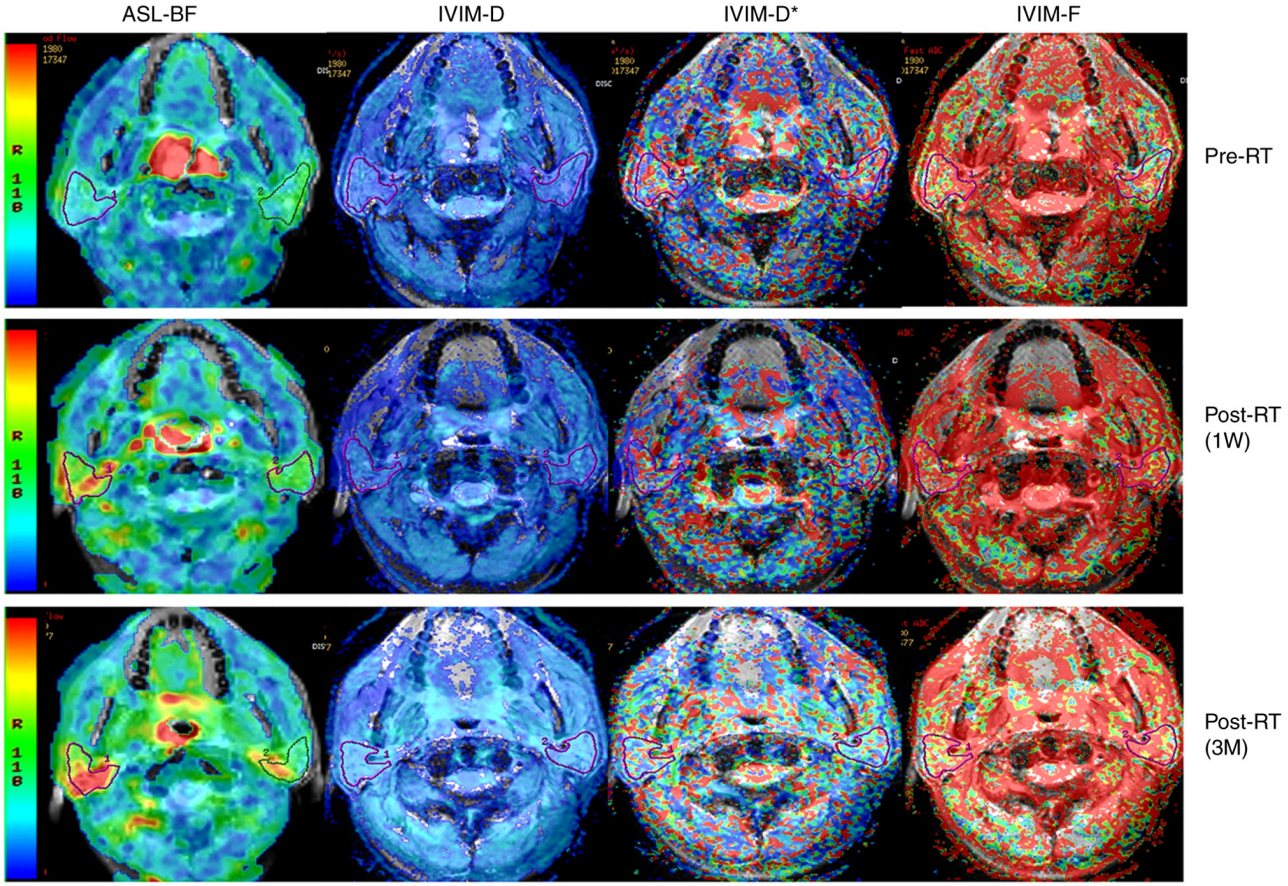

Figure 2. Representative 3D-ASL and IVIM images of bilateral parotid glands of a 58-year-old male patient with nasopharyngeal carcinoma at different time-points pre- and post-RT. For the parotid glands, BF images and D images both illustrated a significantly higher signal at 1W post-RT and 3M post-RT compared to that pre-RT. D* images illustrated a gradually decreasing signal at 1W post-RT and then 3M post-RT compared with that pre-RT. F images illustrated a significantly higher signal at 1W post-RT compared with that pre-RT, and with a similar signal at 3M post-RT. IVIM, intravoxel incoherent motion imaging; D, pure diffusion coefficient; D*, pseudo-diffusion coefficient; F, perfusion fraction; BF, blood flow; ASL, arterial spin labeling; RT, radiotherapy; 1W, 1 week; 3M, 3 months.

imaging techniques sensitive to tissue hemodynamics and cell characteristics are used to clarify the different mechanisms underlying radiation-induced blood vessel and cell damage in healthy tissues. The evaluation and dynamic monitoring of changes in the functional structure of the salivary glands are invaluable during radiation injury. Therefore, the present study used ASL and IVIM technologies to determine the pathological and physiological changes in parotid gland tissue following RT.

Compared with values at baseline pre-RT, the BF value demonstrated a continuous upward trend at 1W, 1M and 3M post-RT. We hypothesized that this trend may be associated with the expansion of microvascular lumen and an increased local blood flow. In the early stages of RT, the number of vascular endothelial cells are significantly decreased, leading to damage to the structure and function of microvessels. This damage may be manifested as abnormal expansion and rupture of the lumen, and other pathological changes (20). The apoptosis of vascular endothelial cells may lead to an inflammatory response in blood vessels (21), and the expression of tumor necrosis factor α and interleukin 1, and other inflammatory factors. Upregulation leads to reactive dilation of microvessels and increased local blood perfusion (20,21). In another study using DCE technology, similar results were

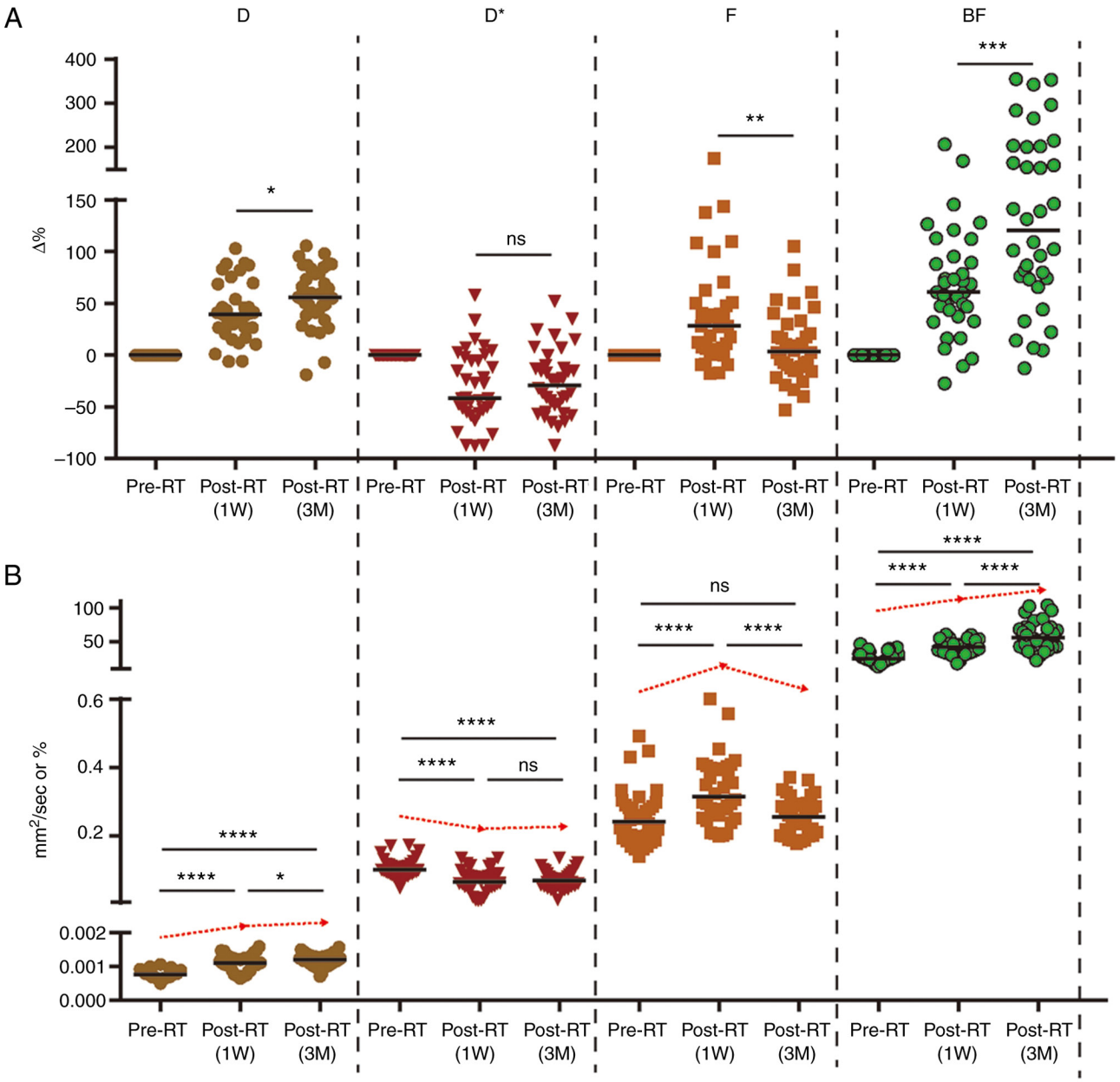

Figure 3. *Dynamic changes of multiple-parameter (D, D*, F and BF) values*. (A) ΔD%, ΔF% and ΔBF% showed significant differences between 1W post-RT and 3M post-RT. (B) Values of D and BF increased significantly after RT at different follow-up time-points. F value increased first and then decreased, while the *D** value was reversed. IVIM, intravoxel incoherent motion imaging; D, pure diffusion coefficient; D*, pseudo-diffusion coefficient; F, perfusion fraction; BF, blood flow; ASL, arterial spin labeling; RT, radiotherapy; ns, non-significant; 1W, 1 week; 3M, 3 months. *P<0.05, **P<0.01, ***P<0.001 and ****P<0.0001.

obtained. The volume transfer constant (K_{trans}) continued to rise following RT, which may be associated with the increase in vascular permeability following early RT (7,22).

Compared with traditional DWI, the IVIM uses a double exponential model to distinguish the signal generated by the diffusion motion of water molecules from the microvascular perfusion signal, to determine an accurate reading of the expansion speed of water molecules in the tissue (23). Results of the present study demonstrated that at 1W and 3M post-RT, the coefficient D value of the parotid gland continued to increase. These results are indicative of the continuous increase in the diffusion rate of water molecules in the parotid gland tissue following RT, supporting the results of previous studies (6,24). Trends observed in the D value are indicative of the gradual shrinkage and degeneration of serous acinar cells of the parotid gland, and these may decrease in number with an increase in the cumulative dose (6,18,22,24). A decrease in the density of glandular cells leads to an increase in the diffusion in tissues. During treatment, internal D gradually increased in the present study. In previous studies, the observation time varied from a few weeks to a few months following RT; however, an increase in the observed D value may be associated with the presence of necrosis and fibrosis (18,24). Moreover, previous studies on DCE MRI demonstrated that an increase in the extracellular space (Ve) and plasma volume (Vp) of the parotid gland tissue following RT may also lead to a significant increase in the free diffusion of water molecules (7,8,22). In the present study, compared with the value observed at baseline, the D* value reflecting the microvascular perfusion component continued to decrease

at 1W and 3M post-RT, while the F-value reflecting the microvessel density increased at 1W post-RT and decreased at 3M post-RT. However, these results were not statistically significant. Notably, these results differed from the change trend of the BF value observed using ASL. We hypothesized that the type of imaging technology may lead to differences, and the histology and cytology of the response also differ. Notably, the diameter and number of capillaries will impact the local BF value. D* and F values are indicative of the number and density of microvessels, and are therefore used more frequently in tumor grading, and in the differentiation between benign and malignant tumors (23,25). Further investigations into the stability of the D* value are required, as this is also affected by vascular osmotic pressure (26). Based on the results of the present study, we hypothesized that the decrease in the number of microvessels in the early stage of RT is not significant, and although there is a transient decrease in the number of microvessels at 3M post-RT, this number remains within a recoverable range.

Results of the present study demonstrated no significant correlation between changes in the parameters of IVIM (ΔD, ΔD* and ΔF) and the average dose received by the parotid glands. These results were similar to those obtained by Marzi *et al* (24). Protecting the parotid gland tissue results in a limited range of dose received by some parotid glands. In addition, differences in parotid gland tissue type, such as fat content, may also affect the results. van Dijk *et al* (27) demonstrated that the ratio of parotid gland fat content to functional parotid gland tissue exerted a positive effect on radiation damage. Previous studies (7,22) also reported the association between average dose and perfusion index (Ve and Vp); however, some studies revealed that the significant correlation between D value and mean dose (Dmean) is closely associated with tissue cell density, which is indicative of a dose-dependent loss of acinar cells (22,24,28). ΔBF is positively correlated with Dmean, and ΔBF_{1W} exhibits a significant correlation with Dmean (24,26,28). Notably, results of the present study demonstrated that there was a trend for BF to increase at 1W and 3M post-RT; however, ΔBF gradually decreased. We hypothesized that some glands may have received higher doses. In the later stage of injury, the effects of inflammation and endothelial destruction are offset by the effects of vascular injury, leading to a decrease in permeability and blood vessel density, which ultimately leads to a decrease in BF. These results are consistent with those described by Lee *et al* (22), and results of the DCE MR study revealed that changes in K_{trans} were consistent.

The present study adopted a prospective research approach to evaluate the values of various functional parameters obtained by MRI, IVIM and ASL in patients with NPC prior to RT, and at 1W and 3M post-RT. Investigating the dynamic changes in various parameters before and after RT at each stage may aid in determining the microscopic changes in parotid gland tissue, including transient pathological changes. Results of the present study may provide novel insights into the mechanisms underlying radiation injury in parotid gland tissue.

However, the present study exhibits numerous limitations. The clinical data of xerostomia (grading of dry mouth and salivary gland secretion) were not included in the present analysis. Therefore, clinical data analysis of parotid gland function was not available in the present study. In addition, the duration of follow-up was limited to 3M post-RT, while salivary gland function may recover up to 5 years after RT (29). The sample size of the present study was small, and factors that may affect parotid gland tissue damage, such as dosage and dose distribution, and differences in parotid gland tissue composition were not classified. Therefore, the results of the present study require further validation in future studies. Moreover, IVIM-DWI and ASL were performed in the present study using parotid gland tissue in the resting state, and investigations were not conducted during the functional state. Thus, further olfactory and taste stimulation studies are required. A combination with ASL technology may lead to improved results.

In conclusion, IVIM-DWI and ASL may aid in determining the mechanisms underlying radiation damage to the parotid gland, through the acquisition and recording of water molecular diffusion, microcirculation and perfusion parameters. Further investigations into the changing trends of D, F and BF values, and the change rate at various follow-up time points may improve the prediction of microstructural changes to parotid gland tissue.

Acknowledgements

Not applicable.

Funding

The present study was supported by the Science Innovative Project of Foshan (grant no. FSOAA-KJ218-1301-0021) and The 14th Five-Year Plan Key Discipline Foundation Of Foshan (grant no. SGSP145036).

Availability of data and materials

The data generated in the present study may be requested from the corresponding author.

Authors' contributions

ZX was responsible for study design, interpretation of data and drafting the manuscript. XZ was responsible for the interpretation of data and drafting the manuscript. YJ, LH, WW, and MG were responsible for the analysis and interpretation of data. XZ, ZX, YJ, LH, WW and MG confirm the authenticity of all the raw data. All authors read and approved the final manuscript.

Ethics approval and consent to participate

The present prospective study was carried out in accordance with the latest version of the Declaration of Helsinki and was approved by the Ethics Committee of The First People's Hospital of Foshan (Foshan, China). All patients provided informed consent to participate in the study.

Patient consent for publication

Not applicable.

Competing interests

The authors declare that they have no competing interests.

References

1. Guo Y, Jiang W, Lakshminarayanan P, Han P, Cheng Z, Bowers M, Hui X, Shpitser I, Siddiqui S, Taylor RH, *et al*: Spatial radiation dose influence on xerostomia recovery and its comparison to acute incidence in patients with head and neck cancer. Adv Radiat Oncol 5: 221-230, 2019.
2. Wang K, Pearlstein KA, Moon DH, Mahbooba ZM, Deal AM, Wang Y, Sutton SR, Motley BB, Judy GD, Holmes JA, *et al*: Assessment of risk of xerostomia after whole-brain radiation therapy and association with parotid dose. JAMA Oncol 5: 221-228, 2019.
3. Zhang T, Liu C, Ma S, Gao Y and Wang R: Protective effect and mechanism of action of rosmarinic acid on radiation-induced parotid gland injury in rats. Dose Response 18: 1559325820907782, 2020.
4. Feng X, Wu Z, Xu J, Xu Y, Zhao B, Pang B, Qu X, Hu L, Hu L, Fan Z, *et al*: Dietary nitrate supplementation prevents radiotherapy-induced xerostomia. Elife 10: e70710, 2021.
5. Xu J, Yan X, Gao R, Mao L, Cotrim AP, Zheng C, Zhang C, Baum BJ and Wang S: Effect of irradiation on microvascular endothelial cells of parotid glands in the miniature pig. Int J Radiat Oncol Biol Phys 78: 897-903, 2010.
6. Fan WJ, Teng F, Luo YR, Yu W, Zhang Q, Lu YP and Ma L: Diffusion-weighted imaging as a follow-up modality for evaluation of major salivary gland function in nasopharyngeal carcinoma patients: A preliminary study. Strahlenther Onkol 196: 530-541, 2020.
7. Juan CJ, Chen CY, Jen YM, Liu HS, Liu YJ, Hsueh CJ, Wang CY, Chou YC, Chai YT, Huang GS and Chung HW: Perfusion characteristics of late radiation injury of parotid glands: Quantitative evaluation with dynamic contrast-enhanced MRI. Eur Radiol 19: 94-102, 2009.
8. Xu Z, Zheng S, Pan A, Cheng X and Gao M: A multiparametric analysis based on DCE-MRI to improve the accuracy of parotid tumor discrimination. Eur J Nucl Med Mol Imaging 46: 2228-2234, 2019.
9. Wu W, Jiang G, Xu Z, Wang R, Pan A, Gao M, Yu T, Huang L, Quan Q and Li J: Three-dimensional pulsed continuous arterial spin labeling and intravoxel incoherent motion imaging of nasopharyngeal carcinoma: Correlations with Ki-67 proliferation status. Quant Imaging Med Surg 11: 1394-1405, 2021.
10. Li Y, Lin CY, Qi YF, Wang X, Chen B, Zhou HL, Ren J, Yang JJ, Xiang Y, He YL, *et al*: Three-dimensional turbo-spin-echo amide proton transfer-weighted and intravoxel incoherent motion MR imaging for type I endometrial carcinoma: Correlation with Ki-67 proliferation status. Magn Reson Imaging 78: 18-24, 2021.
11. Yu YM, Wang W, Wen J, Zhang Y, Lu GM and Zhang LJ: Detection of renal allograft fibrosis with MRI: Arterial spin labeling outperforms reduced field-of-view IVIM. Eur Radiol 31: 6696-6707, 2021.
12. Poynton CB, Lee MM, Li Y, Laszik Z, Worters PW, Mackenzie JD and Courtier J: Intravoxel incoherent motion analysis of renal allograft diffusion with clinical and histopathological correlation in pediatric kidney transplant patients: A preliminary cross-sectional observational study. Pediatr Transplant 21: e12996, 2017.
13. Jia QJ, Zhang SX, Chen WB, Liang L, Zhou ZG, Qiu QH, Liu ZY, Zeng QX and Liang CH: Initial experience of correlating parameters of intravoxel incoherent motion and dynamic contrast-enhanced magnetic resonance imaging at 3.0 T in nasopharyngeal carcinoma. Eur Radiol 24: 3076-3087, 2014.
14. Kang M, Zhou P, Li G, Yan H and Wang R: Validation of the 8th edition of the UICC/AJCC staging system for nasopharyngeal carcinoma treated with intensity-modulated radiotherapy. Oncotarget 8: 70586-70594, 2017.
15. Chinese Committee for Staging of Nasopharyngeal Carcinoma: The 2017 edition for staging of nasopharyngeal carcinoma in China (The Chinese 2008 expert consensus on staging revision of nasopharyngeal carcinoma).Chinese J Radiation Oncology, 26: 1119-1124, 2017 (In Chinese).
16. Westgaard KL, Hynne H, Amdal CD, Young A, Singh PB, Chen X, Rykke M, Hove LH, Aqrawi LA, Utheim TP, *et al*: Oral and ocular late effects in head and neck cancer patients treated with radiotherapy. Sci Rep 11: 4026, 2021.
17. Acauan MD, Figueiredo MA, Cherubini K, Gomes AP and Salum FG: Radiotherapy-induced salivary dysfunction: Structural changes, pathogenetic mechanisms and therapies. Arch Oral Biol 60: 1802-1810, 2015.
18. Wu VWC, Ying MT, Kwong DL, Khong PL, Wong GK and Tam SY: A longitudinal study on parotid and submandibular gland changes assessed by magnetic resonance imaging and ultrasonography in post-radiotherapy nasopharyngeal cancer patients. BJR Open 2: 20200003, 2020.
19. Hu S, Gao Y, Zhou H, Kong F, Xiao F, Zhou P and Chen Y: New insight into mitochondrial changes in vascular endothelial cells irradiated by gamma ray. Int J Radiat Biol 93: 470-476, 2017.
20. Fajardo LF: The pathology of ionizing radiation as defined by morphologic patterns. Acta Oncol 44: 13-22, 2005.
21. Boström M, Kalm M, Eriksson Y, Bull C, Ståhlberg A, Björk-Eriksson T, Hellström Erkenstam N and Blomgren K: A role for endothelial cells in radiation-induced inflammation. Int J Radiat Biol 94: 259-271, 2018.
22. Lee FK, King AD, Kam MK, Ma BB and Yeung DK: Radiation injury of the parotid glands during treatment for head and neck cancer: Assessment using dynamic contrast-enhanced MR imaging. Radiat Res 175: 291-296, 2011.
23. Bisdas S, Koh TS, Roder C, Braun C, Schittenhelm J, Ernemann U and Klose U: Intravoxel incoherent motion diffusion-weighted MR imaging of gliomas: Feasibility of the method and initial results. Neuroradiology 55: 1189-1196, 2013.
24. Marzi S, Forina C, Marucci L, Giovinazzo G, Giordano C, Piludu F, Landoni V, Spriano G and Vidiri A: Early radiation-induced changes evaluated by intravoxel incoherent motion in the major salivary glands. J Magn Reson Imaging 41: 974-982, 2015.
25. Shen N, Zhao L, Jiang J, Jiang R, Su C, Zhang S, Tang X and Zhu W: Intravoxel incoherent motion diffusion-weighted imaging analysis of diffusion and microperfusion in grading gliomas and comparison with arterial spin labeling for evaluation of tumor perfusion. J Magn Reson Imaging 44: 620-632, 2016.
26. Dolgorsuren EA, Harada M, Kanazawa Y, Abe T, Otomo M, Matsumoto Y, Mizobuchi Y and Nakajima K: Correlation and characteristics of intravoxel incoherent motion and arterial spin labeling techniques versus multiple parameters obtained on dynamic susceptibility contrast perfusion MRI for brain tumors. J Med Invest 66: 308-313, 2019.
27. van Dijk LV, Thor M, Steenbakkers RJHM, Apte A, Zhai TT, Borra R, Noordzij W, Estilo C, Lee N, Langendijk JA, *et al*: Parotid gland fat related Magnetic Resonance image biomarkers improve prediction of late radiation-induced xerostomia. Radiother Oncol 128: 459-466, 2018.
28. Zhang L, Murata Y, Ishida R, Ohashi I, Yoshimura R and Shibuya H: Functional evaluation with intravoxel incoherent motion echo-planar MRI in irradiated salivary glands: A correlative study with salivary gland scintigraphy. J Magn Reson Imaging 14: 223-229, 2001.
29. Hey J, Setz J, Gerlach R, Janich M, Hildebrandt G, Vordermark D, Gernhardt CR and Kuhnt T: Parotid gland-recovery after radiotherapy in the head and neck region-36 months follow-up of a prospective clinical study. Radiat Oncol 6: 125, 2011.